Academic Journal of Science and Technology
ISSN: 2771-3032 | Vol. 14, No. 3, 2025

Optimization of SINS / GNSS Integrated Navigation Model Based on Prior Information

Yu Sun[1, a]

[1]School of Geomatics and Urban Spatial Informatics, Beijing University of Civil Engineering and Architecture, Beijing 102616, China
[a]2108160122007@stu.bucea.edu.cn

Highlights: 1. Extraction of information from inertial navigation data with a second-order Butterworth low-pass filter. 2. Employing a priori information to enhance the reliability of results in combinatorial navigation through the process of combinatorial solving. 3. Estimation of Integrated Navigation Parameters Utilizing Kalman Filtering.

Abstract: Inertial navigation systems (INS) are extensively utilized across various domains due to their independence from external information during operation, commendable autonomy and stealth, and capability to deliver comprehensive data output. The loose combination navigation of SINS/GNSS benefits from the complementing function of the Global Navigation Satellite System (GNSS), characterized by its straightforward principle and ease of implementation through the integration of GNSS data with the auxiliary correction provided by INS data. This work addresses the error issue in inertial navigation by proposing a filtering method utilizing a second-order Butterworth low-pass filter to extract a priori information from the inertial navigation data. Subsequently, it examines the impact of including a priori information on the efficacy of the SINS/GNSS loose-combination navigation. The findings indicate that incorporating a priori information can effectively rectify navigation trajectory deviations, enhance the convergence rate of misalignment angle errors, expedite the convergence of three-dimensional velocity errors in the northeastern sky, and diminish the amplitude of position error fluctuations. The precision of SINS/GNSS loose combination navigation is markedly enhanced.

Keywords: SINS, GNSS, loose combination, prior information.

1. Introduction

In recent years, the rapid development of high-performance and low-cost MEMS inertial sensors[1] has significantly expanded the application areas of inertial navigation systems[2-5]. The loose combination method based on MEMS inertial navigation system (SINS) and global satellite navigation system (GNSS) has been widely used in many fields[6-7]. However, in real-time applications, the method still has some limitations[8], and in environments such as urban canyons where GNSS signals are susceptible to occlusion or interference[9], standalone navigation systems relying only on MEMS inertial sensors have errors that accumulate rapidly as the interruption of GNSS signals lengthens[10]. To cope with the above problems, the loose combination method of inertial navigation and satellite navigation usually employs an Extended Kalman Filter (EKF) [11-12]. However, this method assumes that both system dynamics and observation noise are known white noise[13], whereas, in practice, the noise of MEMS inertial devices is usually time-dependent, i.e., colored noise, which has more complex properties[14-15]. Reducing the system dynamics noise to white noise for processing may lead to a mismatch between the computed covariance matrix of the Kalman filter output and the actual noise characteristics, which triggers a bias in the error model[16-18]. limiting the accuracy improvement of the loose combination approach of inertial navigation and satellite navigation is constrained[19-20]. This work proposes the utilization of a second-order Butterworth low-pass filter to process SINS data, thereby eliminating high-frequency noise interference and extracting a priori information for inertial navigation. A priori information is incorporated into the loose combination solution procedure of SINS and GNSS to enhance positioning accuracy as illustrated in Figure 1.

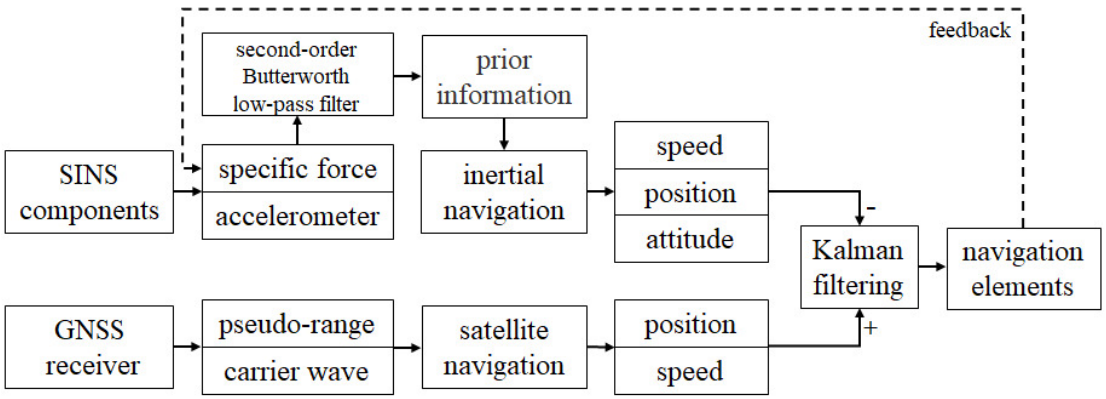

Figure 1. Flow chart of SINS / GNSS integrated navigation model based on prior information

2. Integrated Navigation Based on Prior Information

2.1. Second-order Butterworth low-pass filter

The second-order Butterworth filter is extensively utilized in signal processing because of its characteristic of maximum flatness. It is primarily defined by a flat amplitude-frequency response in the passband, which progressively diminishes to zero in the stopband and displays a gradual transition band around the cutoff frequency. This attribute allows the second-order Butterworth filter to efficiently eliminate high-frequency noise while maintaining the fidelity of the low-frequency signal to the greatest extent possible. The second-order Butterworth filter functions as a low-pass filter, permitting low-frequency signals to pass with minimal attenuation while substantially rejecting higher frequency signals, therefore efficiently reducing high-frequency noise interference. The transfer function is represented by the following mathematical expression:

$$H(s)=\frac{V_2(s)}{V_1(s)}=\frac{KC\omega_c^2}{s^2+B\omega_c s+C\omega_c^2} \tag{1}$$

where K represents the gain, ω_c is the cut-off frequency, B and C denote the normalization factors.

2.2. PINS/GNSS integrated navigation

The fundamental notion of the SINS/GNSS loose combination is illustrated in Figure 2. During the resolution process, satellite navigation (GNSS) and inertial navigation (INS) operate independently, after which the GNSS output data is utilized to provide auxiliary corrections to the INS results, thereby significantly enhancing positioning accuracy, characterized by a succinct theoretical framework and ease of implementation.

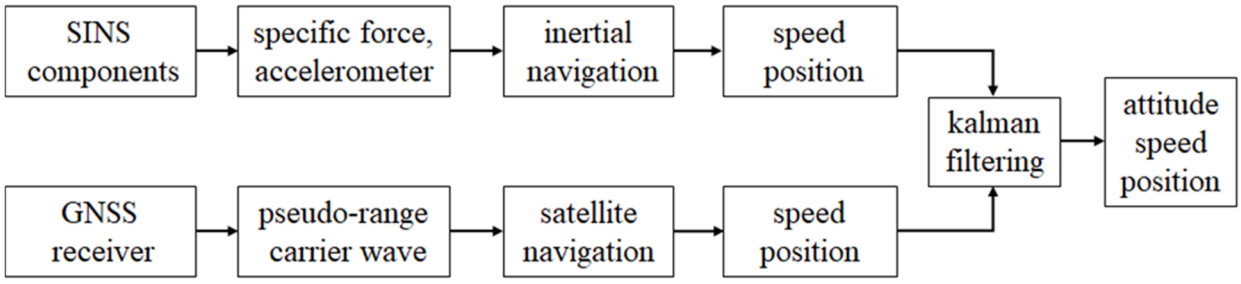

Figure 2. Flow chart of SINS/GNSS loose integration

The inertial navigation system computes component output data to derive velocity and position information, while the GNSS receiver utilizes satellite navigation to acquire corresponding velocity and position data. Thereafter, the velocity and position data acquired from the independent solutions of inertial navigation and satellite navigation are processed separately, and the results are input into the Kalman filter for error correction. The Kalman filter processing yields high-precision data on location, velocity, and attitude. The state equation for the loose combination of SINS and GNSS is presented below:

$$\dot{\boldsymbol{X}}_k(t)=\boldsymbol{F}_k(t)\boldsymbol{X}_k(t)+\boldsymbol{G}_k(t)\boldsymbol{W}_k(t) \tag{1}$$

Expansion formulas for the loose combination equation of state are derived by modeling the inaccuracies of the SINS accelerometer and gyroscope elements, as well as the errors in velocity, position, attitude, and GNSS receiver clock discrepancies:

$$\begin{bmatrix}\dot{\boldsymbol{f}}^n\\ \delta\dot{\boldsymbol{v}}^n\\ \delta\dot{\boldsymbol{\gamma}}^n\\ \dot{\boldsymbol{b}}_g^b\\ \dot{\boldsymbol{b}}_a^b\end{bmatrix}=\begin{bmatrix}\boldsymbol{F}_{ff} & \boldsymbol{F}_{fV} & \boldsymbol{F}_{f\gamma} & -\boldsymbol{C}_b^n & \boldsymbol{0}\\ \boldsymbol{F}_{Vf} & \boldsymbol{F}_{VV} & \boldsymbol{F}_{V\gamma} & \boldsymbol{0} & \boldsymbol{C}_b^n\\ \boldsymbol{0} & \boldsymbol{F}_{\gamma V} & \boldsymbol{F}_{\gamma\gamma} & \boldsymbol{0} & \boldsymbol{0}\\ \boldsymbol{0} & \boldsymbol{0} & \boldsymbol{0} & \boldsymbol{0} & \boldsymbol{0}\\ \boldsymbol{0} & \boldsymbol{0} & \boldsymbol{0} & \boldsymbol{0} & \boldsymbol{0}\end{bmatrix}\begin{bmatrix}\boldsymbol{f}^n\\ \delta\boldsymbol{v}^n\\ \delta\boldsymbol{\gamma}^n\\ \boldsymbol{b}_g^b\\ \boldsymbol{b}_a^b\end{bmatrix}+\begin{bmatrix}-\boldsymbol{C}_b^n & \boldsymbol{0}\\ \boldsymbol{0} & \boldsymbol{C}_b^n\\ \boldsymbol{0} & \boldsymbol{0}\\ \boldsymbol{0} & \boldsymbol{0}\\ \boldsymbol{0} & \boldsymbol{0}\end{bmatrix}\begin{bmatrix}\boldsymbol{\omega}_g^b\\ \boldsymbol{\omega}_a^b\end{bmatrix} \tag{2}$$

Where each element is a matrix, $\boldsymbol{0}$ signifies the all-zero matrix; $\boldsymbol{f}^n$, $\boldsymbol{\delta}$, $\boldsymbol{v}^n$, $\boldsymbol{\delta\gamma}^n$, $\boldsymbol{b}_g^b$ and $\boldsymbol{b}_a^b$ is the state transfer matrix of attitude, velocity, and position errors of the three axes. C_b^n is the noise allocation matrix.

An independent solution derived from inertial guidance, the guard guide velocity, and position equations is utilized as input to the system. Following the processing of the range to the SINS data for correction, the measurement equations for the SINS/GNSS loose combination are as follows:

$$\boldsymbol{Z}(t)=\boldsymbol{H}(t)\cdot\boldsymbol{X}(t)+\boldsymbol{V}(t) \tag{3}$$

Where $\boldsymbol{Z}(t)$ represents the system measurement, $\boldsymbol{H}(t)$ denotes the system measurement matrix, and $\boldsymbol{V}(t)$ signifies the system measurement white noise. The three-dimensional coordinates have been recorded, returning the following results:

$$\boldsymbol{Z}(t)=\begin{bmatrix}\boldsymbol{l}_{SINS}-\boldsymbol{l}_{GPS}\\ \boldsymbol{\lambda}_{SINS}-\boldsymbol{\lambda}_{GPS}\\ \boldsymbol{h}_{SINS}-\boldsymbol{h}_{GPS}\end{bmatrix}=\begin{bmatrix}(r_N+\boldsymbol{h})cos\boldsymbol{\varphi}(\boldsymbol{\lambda}_{SINS}-\boldsymbol{\lambda}_{GPS})\\ (\boldsymbol{r}_M+\boldsymbol{h})(\boldsymbol{\varphi}_{SINS}-\boldsymbol{\varphi}_{GPS})\\ \boldsymbol{h}_{SINS}-\boldsymbol{h}_{GPS}\end{bmatrix} \tag{4}$$

Utilizing the state and measurement equations of the SINS/GNSS loose combination, Kalman filtering assigns weights to the corrections of the state and actual measurements predicted at that instant, based on available information, to derive the optimal estimate of the subsequent output that satisfies the criterion. Kalman filtering discretizes the content; hence, the continuous state and measurement equations are discretized prior to application, employing a Taylor series expansion for this purpose:

$$\begin{cases} X_k = \Phi_{k,k-1} X_{k-1} + W_{k-1} \\ Z_k = H_k K_k + v_k \end{cases} \tag{5}$$

Where X_k represents the state vector at time k, $\Phi_{k,k-1}$ denotes the one-step transfer matrix of the state at two consecutive moments, W signifies the system excitation noise, Z_k indicates the measurement vector, H_k refers to the measurement matrix, and v stands for the measurement noise.

The fundamental equation of Kalman filtering comprises five essential components: one-step state prediction, mean square error of one-step state prediction, filtering gain, state estimation, and mean square error of state estimation. Kalman filtering employs the initial value and its associated estimation error to perform iterative calculations through the time update and measurement update processes, thereby continuously refining the optimal estimation of the system state. The fundamental equations of Kalman filtering are presented below:

$$\hat{X}_{k,k-1} = \Phi_{k,k-1} \hat{X}_{k-1} \tag{6}$$

$$\Pi_{\kappa,\kappa-1} = \Phi_{\kappa,\kappa-1} \Pi_{\kappa-1} \Phi^T_{\kappa,\kappa-1} + \upsilon_{\kappa-1} \tag{7}$$

$$K_k = P_{k,k-1} H_k^T \left(H_k P_{k,k-1} H_k^T + R_k \right)^{-1} \tag{8}$$

$$\hat{X}_k = \hat{X}_{k,k-1} + K_k \left(Z_k - H_k \hat{X}_{k,k-1} \right) \tag{9}$$

$$P_k = \left(I - K_k H_k \right) P_{k,k-1} \tag{10}$$

3. Experiment and Result

3.1. Simulated data

This work is founded on the implementation of the open-source PINS algorithm. The flight trajectory data are simulated using parameter settings. Forty seconds after activation and remaining stationary, ascend in the true north direction with an acceleration of 1 m/s² for ten seconds, thereafter maintaining a constant velocity for one hundred seconds; execute a left turn of ninety degrees and sustain a constant speed for seventy seconds; perform a right turn of two hundred seventy degrees and maintain a constant speed for fifty seconds; execute a left turn of ninety degrees followed by a right turn of four hundred fifty degrees, sustaining a constant speed for one hundred thirty seconds; replicate the aforementioned trajectory three times to establish the flight path. The optimal flying path is determined by configuring the attitude and position parameters, as seen in Fig. 3. The initial position is indicated by a red five-star in the illustration, with the relative position described corresponding to the coordinates (0, 0, 0). The trajectory proceeds in the true north direction until its conclusion.

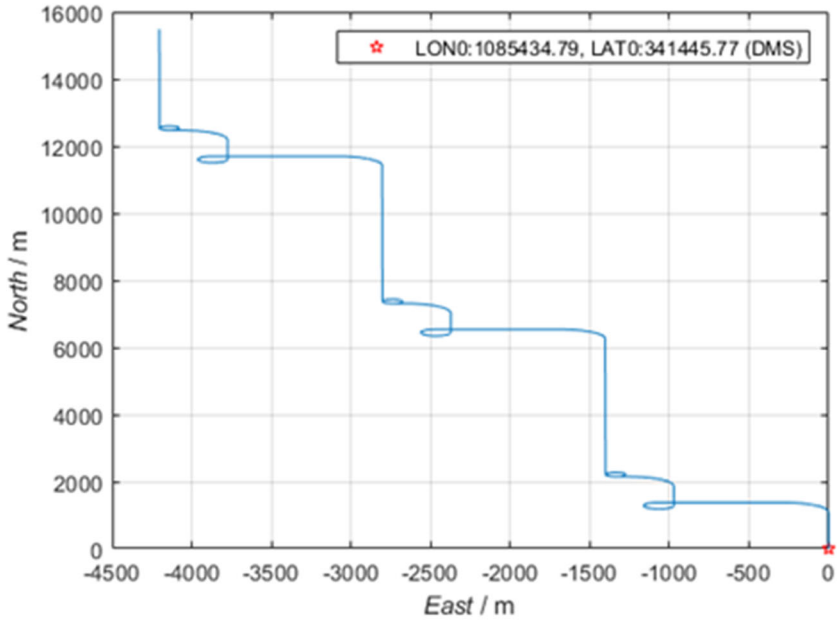

Figure 3. Simulation of ideal flight trajectory

In real-world scenarios, the utilization of equipment containing inertial components for flight testing is subject to numerous errors. Therefore, it is essential to integrate the actual conditions with an ideal trajectory simulation by incorporating the relevant error models. This includes the zero bias of the gyroscope, zero bias of the accelerometer, random drift of the gyroscope, random drift of the accelerometer's speed, as well as the initial trajectory misalignment angle error, speed error, position error, and other error terms to accurately replicate the authentic flight environment. The flight path is depicted in Fig. 4.

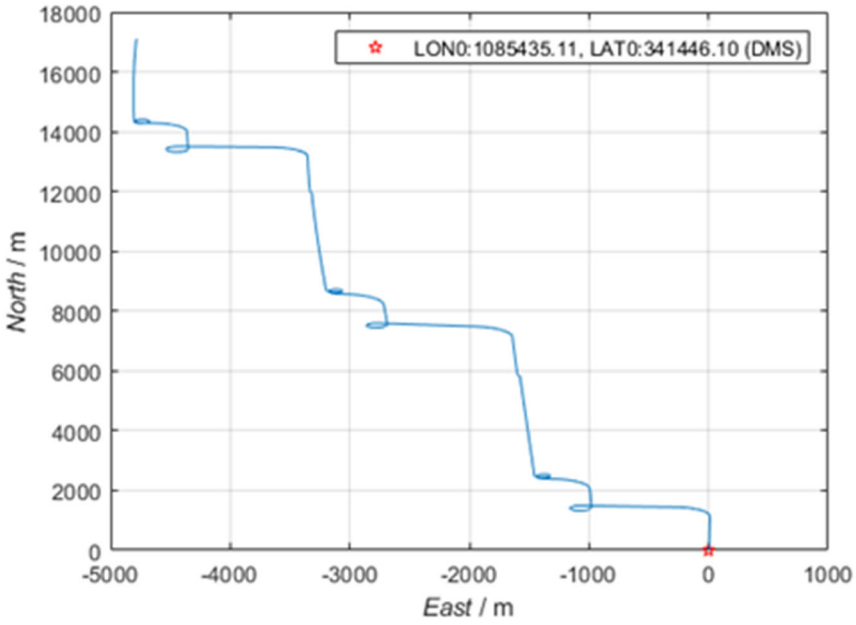

Figure 4. Inertial navigation flight trajectory

3.2. Prior information processing

A second-order Butterworth low-pass filter is employed to handle the IMU data, effectively eliminating high-frequency noise interference. The filter cut-off frequency correlates with the FFT of the original data; based on empirical evidence, attempt to establish cut-off frequencies of 30 Hz, 40 Hz, 50 Hz, and 60 Hz to filter the data, compare the results from these four trials, and ascertain the optimal cut-off frequency. The experimental sampling frequency is 200 Hz, the cut-off frequency is 60 Hz, and a second-order Butterworth filter is employed to process the IMU raw data. Figure 5 illustrates the outcomes of the IMU data processed using the second-order Butterworth filter.

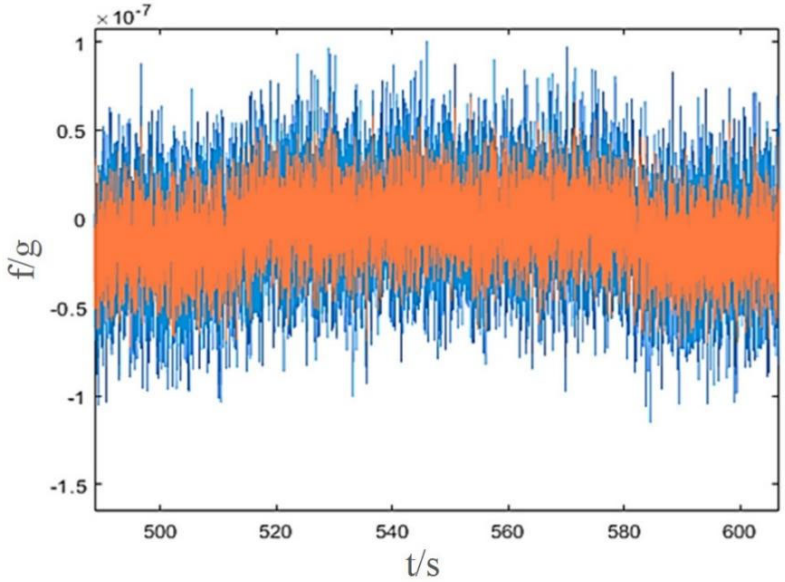

Figure 5. Second-order Butterworth low-pass filtering results

3.3. Prior information aided PINS/GNSS integrated navigation

The flight path analyzed by combined navigation is depicted in Fig. 6. In comparison to the flight trajectory of inertial navigation, combined navigation exhibits superior corrective efficacy, aligning more closely with the ideal flying trajectory.

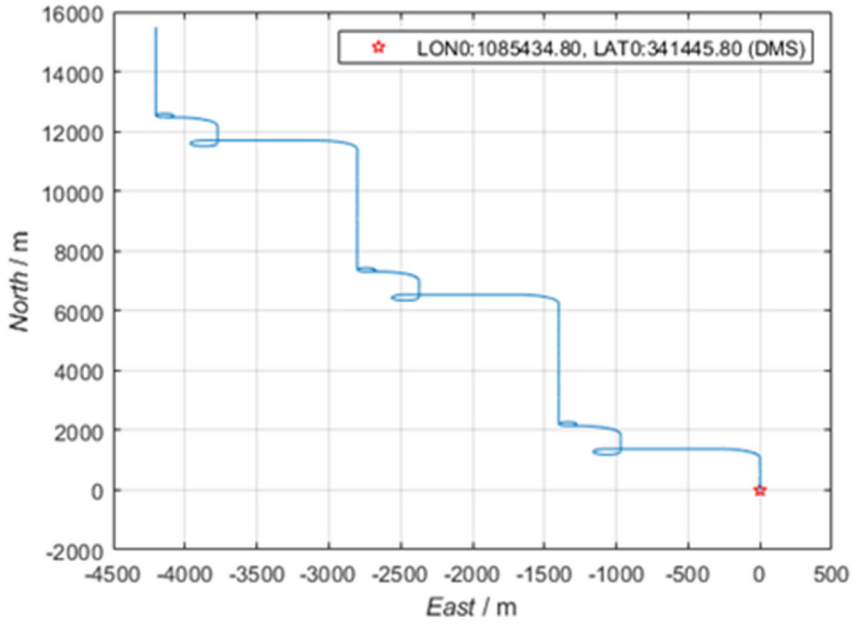

Figure 6. SINS / GNSS integrated navigation flight trajectory

The second-order Butterworth low-pass filter effectively corrects the misalignment angle offset in the combined SINS/GNSS navigation system. Figures 7 and 8 illustrate the changes in misalignment angle in combined navigation, both prior to and following the filter processing. The initial value of the misalignment angle is established at 20 minutes. In the combined navigation prior to filtering, the misalignment angle shows convergence from this initial value after 500 seconds, ultimately reaching a peak of approximately 26 minutes. Conversely, the misalignment angle in the combined navigation post-filtering converges after 390 seconds, achieving a maximum value of around 22 minutes. The convergence speed of the misalignment angle after filtering shows a 30% increase compared to the misalignment angle of the combined navigation prior to filtering, indicating a significant enhancement in convergence speed.

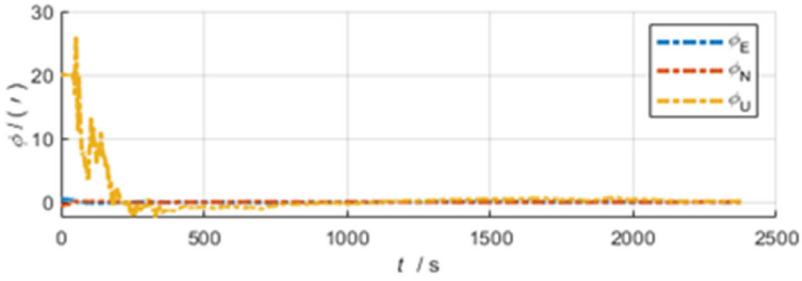

Figure 7. The variation of misalignment angle error of the original integrated navigation

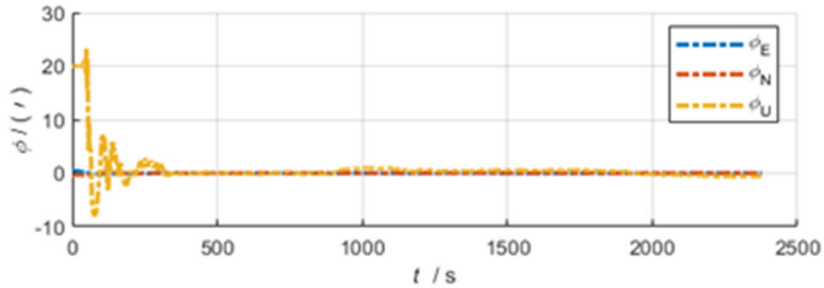

Figure 8. The variation of misalignment angle error of integrated navigation solution with prior information

The alterations in combined navigation velocity errors prior to and following the filtering of IMU data are illustrated in Figs. 9 and 10. The eastward velocity error prior to filtering stabilizes after 493 seconds, consistently falling within the interval of [-0.04, 0.04] m/s. Similarly, the northward velocity error reaches convergence after 440 seconds, also remaining within the range of [-0.04, 0.04] m/s. The skyward velocity error achieves convergence after 413 seconds. The values converge and continue to fluctuate within the range of [-0.01, 0.01] m/s, while the upward velocity error stabilizes after 413 seconds, maintaining variations within the same range of [-0.01, 0.01] m/s. The filtered combined navigation results

show convergence after 300 seconds for the eastward velocity error, maintaining a variation within the range of [-0.04, 0.04] m/s. Convergence occurs after 410 seconds for the northward velocity error, with variations in the range of [-0.03, 0.04] m/s. Finally, convergence is achieved after 443 seconds for the skyward velocity error, which varies within the range of [-0.01, 0.01] m/s. The navigation velocity error, once filtered, demonstrates a quicker convergence and exhibits a reduced oscillation range.

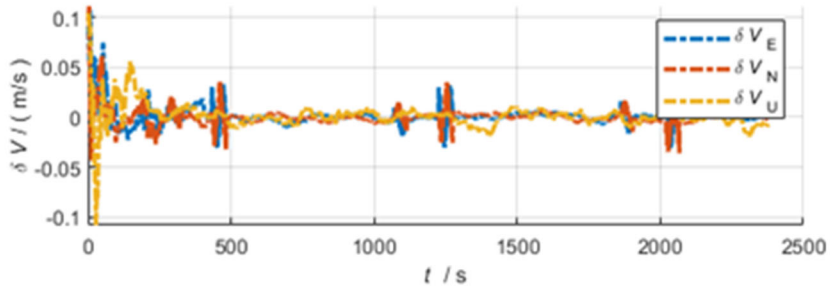

Figure 9. The variation of velocity error in the original integrated navigation solution

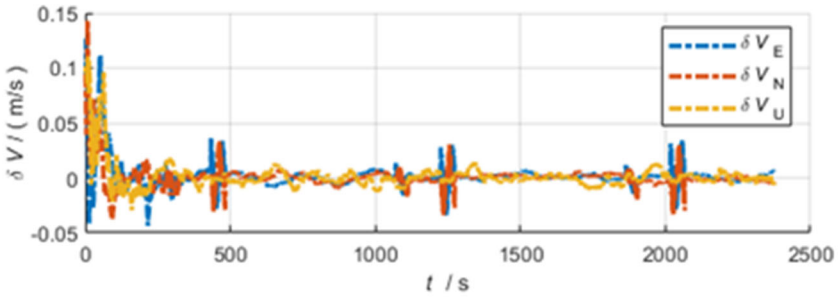

Figure 10. The variation of velocity error in the integrated navigation solution with prior information

The variations in position inaccuracy are illustrated in Figures 111 and 12. The positions of combined navigation exhibited continuous fluctuations before and after filtering, following rapid convergence; however, the fluctuation ranges differed. Prior to data filtering, the initial error in the elevation direction reached 4m, oscillating within the range of [-1.8, 1.5]m post-convergence. In contrast, the elevation direction error of the combined navigation subjected to filtering oscillated within [-1.2, 1.3]m. Consequently, the fluctuation of the combined navigation position error was reduced by 75.76% after the filtering process. The combined navigation elevation direction error post-filtering oscillates between [-1.2, 1.3]m, while the variation of the combined navigation position error is diminished by 75.76% following the filtering process.

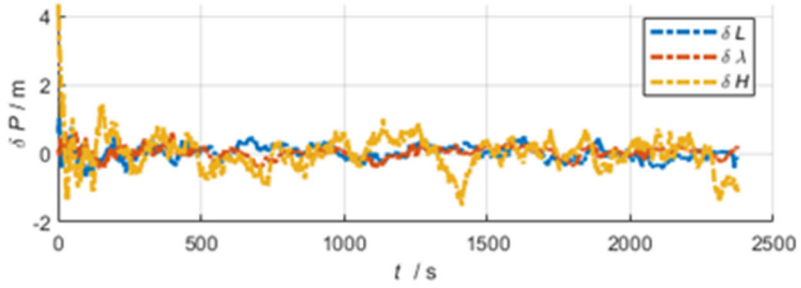

Figure 11. The variation of position error in the original integrated navigation solution

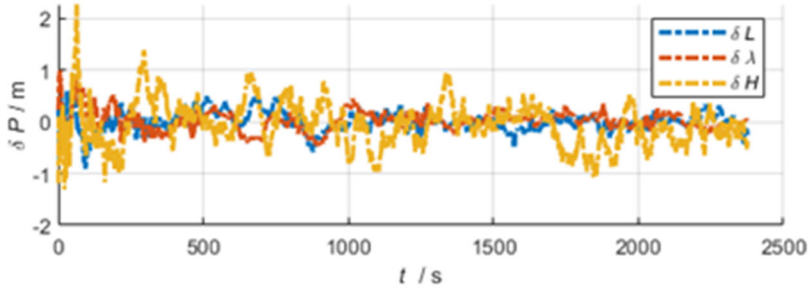

Figure 12. The variation of position error in the integrated navigation solution with prior information

In the context of SINS/GNSS loose combination navigation, employing a second-order Butterworth low-pass filter to process the initial IMU data significantly influences the navigation outcomes. Simulation results indicate that the original SINS/GNSS combination navigation results, following the a priori information processing of the navigation misalignment angle, exhibit a 30% increase in convergence speed, demonstrating a marked enhancement in convergence rate. The convergence speed of the speed error is typically enhanced, the oscillation range is diminished, and the position error fluctuation is reduced by 75.76%.

4. Conclusion

This work examines the pretreatment of IMU data to produce a priori knowledge within the context of SINS/GNSS combined navigation, evaluates its influence on the navigation outcomes, and analyzes the results of SINS/GNSS loose combined navigation solutions both before to and following filter processing. The simulation findings indicate that the SINS/GNSS integrated navigation utilizing a priori information may proficiently rectify the flight trajectory. In comparison to the original combined navigation results, the combined navigation utilizing a priori information exhibits expedited convergence of the misalignment angle error, enhanced convergence of the velocity error across the three northeast sky directions, reduced fluctuation range of the position error, and a significant enhancement in navigation accuracy.

5. Conflicts of Interest

The authors declare no conflict of interest.

References

[1] Borodacz, K., Szczepański, C., & Popowski, S. (2021). Review and selection of commercially available IMU for a short time inertial navigation. Aircraft Engineering and Aerospace Technology.

[2] Lyu P., Wang B., Lai J., Bai S., Liu M., Yu W. (2023), A factor graph optimization method for high-precision IMU-based navigation system, IEEE Transactions on Instrumentation and Measurement, Vol. 72, pp. 1-12.

[3] Mahdi A. E., Azouz A., Abdalla A. E., Abosekeen A. (2022), IMU-Error Estimation and Cancellation Using ANFIS for Improved UAV Navigation, Proceedings of the 2022 13th International Conference on Electrical Engineering (ICEENG), pp. 120-124.

[4] Sun M., Wang Y., Joseph W., Plets D. (2022), Indoor Localization Using Mind Evolutionary Algorithm-Based Geomagnetic Positioning and Smartphone IMU Sensors, IEEE Sensors Journal, Vol. 22, No. 7, pp. 7130-7141.

[5] Xu R., Chen S., Bai S., Wen W. (2024), Nonlinearity-Aware ZUPT-Aided Pedestrian Inertial Navigation Based on Cubature Kalman Filter in Urban Canyons, IEEE Transactions on Instrumentation and Measurement, Vol. 73, pp. 1-15.

[6] Ibrahim A., Abosekeen A., Azouz A., Noureldin A. (2023), Enhanced Autonomous Vehicle Positioning Using a Loosely Coupled INS/GNSS-Based Invariant-EKF Integration, Sensors, Vol. 23, No. 13, Article No. 6097.

[7] Zhu F., Cai Q., Tao X., Zhang X., Liu W. (2024), POSMind: developing a hierarchical GNSS/SINS post-processing service system for precise position and attitude determination, GPS Solut., Vol. 28, No. 3, pp. 1-21.

[8] Chen Q., Zhang Q., Niu X., Liu J. N. (2021), Semi-analytical assessment of the relative accuracy of the GNSS/INS in railway track irregularity measurements, Satellite Navigation, Vol. 2, pp. 1-16.

[9] Yao Y., Xu X., Zhu C., Chan C.-Y. (2017), A hybrid fusion algorithm for GPS/INS integration during GPS outages, Measurement, Vol. 103, pp. 42-51.

[10] Mahdi A. E., Azouz A., Abdalla A. E., Abosekeen A. (2022), A Machine Learning Approach for an Improved Inertial Navigation System Solution, Sensors, Vol. 22, No. 4, Article No. 1687.

[11] Damagatla R. K., Atia M. (2024), Improving EKF-Based IMU/GNSS Fusion Using Machine Learning for IMU Denoising, IEEE Access, Vol. 12, pp. 114358-114369.

[12] Liu J., Guo G. (2021), Vehicle Localization During GPS Outages With Extended Kalman Filter and Deep Learning, IEEE Transactions on Instrumentation and Measurement, Vol. 70, pp. 1-10.

[13] Iyer K., Dey A., Xu B., Sharma N., Hsu L.-T. (2024), Enhancing Positioning in GNSS Denied Environments Based on an Extended Kalman Filter Using Past GNSS Measurements and IMU, IEEE Transactions on Vehicular Technology, Vol. 73, No. 6, pp. 7908-7924.

[14] Groves P. (2007), Principles of GNSS, Inertial, and Multisensor Integrated Navigation Systems.

[15] Chang L., Luo Y. (2023), Log-Linear Error State Model Derivation Without Approximation for INS, IEEE Transactions on Aerospace and Electronic Systems, Vol. 59, No. 2, pp. 2029-2035.

[16] Luo Y., Lu F., Guo C., Liu J. (2024), Matrix Lie Group-Based Extended Kalman Filtering for Inertial-Integrated Navigation in the Navigation Frame, IEEE Transactions on Instrumentation and Measurement, Vol. 73, pp. 1-16.

[17] Wang J., Chen W., Weng D. (2025), GNSS/IMU/map-matching feedback integration with adaptive GNSS accuracy estimation by using low-quality sensors for vehicle localization in urban canyon, Measurement, Vol. 240, pp. 115541.

[18] Nassar S., El-Sheimy N. (2006), A Combined Algorithm of Improving INS Error Modeling and Sensor Measurements for Accurate INS/GPS Navigation, GPS Solutions, Vol. 10, pp. 29-39.

[19] Lyu P., Wang B., Lai J., Bai S., Liu M., Yu W. (2023), A Factor Graph Optimization Method for High-Precision IMU-Based Navigation System, IEEE Transactions on Instrumentation and Measurement, Vol. 72, pp. 1-12.

[20] Tang J., Bian H., Ma H., Wang R. (2024), SINS/GNSS Integrated Navigation Based on Invariant Error Models in Inertial Frame, IEEE Sensors Journal, Vol.